THE JOURNAL OF PHYSICAL CHEMISTRY B

Feature Article

pubs.acs.org/JPCB

# Understanding the Rates and Molecular Mechanism of Water-Exchange around Aqueous Ions Using Molecular Simulations

Harsha V. R. Annapureddy and Liem X. Dang*

Physical Sciences Division, Pacific Northwest National Laboratory, Richland, Washington 93352, United States

**ABSTRACT:** Solvation processes occurring around aqueous ions are of fundamental importance in physics, chemistry, and biology. Over the past few decades, several experimental and theoretical studies were devoted to understanding ion solvation and the processes involved in it. In this article, we present a summary of our recent efforts that, through computer simulations, focused on providing a comprehensive understanding of solvent-exchange processes around aqueous ions. To accomplish these activities, we have looked at the mechanistic properties associated with the water-exchange process, such as potentials of mean force, time-dependent transmission coefficients, and the corresponding rate constants using transition state theory, the reactive flux method, and Grote−Hynes treatments of the dynamic response of the solvent.

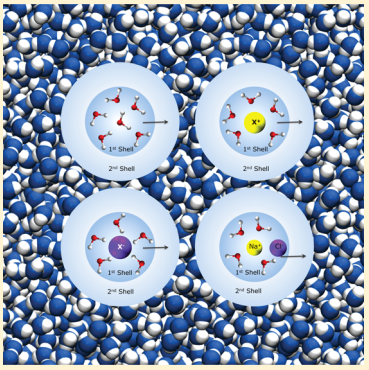

## 1. INTRODUCTION

Aqueous ions are ubiquitous in physics, chemistry, and biology. Our understanding of the importance of their role in many electrochemical and biological processes is continuously growing. As a result, there is a great demand for detailed fundamental knowledge and molecular-level understanding of ion hydration and the processes involved in it. Minor differences in ion properties could cause major changes in their role in biological processes. To fully understand these effects, expert knowledge of the nanostructure of the hydrated ions and their dynamical characteristics is necessary. In the past few decades, significant amounts of research efforts have been dedicated to understanding various properties such as hydration structure and the thermodynamic aspects of ion solvation.

Several studies on thermodynamics of ion solvation and hydration structure are reported in the literature for variety of ions. In this article, we restrict the discussion to only ion cases that are relevant to the current study. Experimental techniques used to study the hydration structure include X-ray diffraction, neutron diffraction, and X-ray absorption spectroscopy (for more information see review by Ohtaki et al.[1]). Soper et al. used neutron diffraction experiments to study hydration structure round the halide and hydroxyl anions.[2,3] Using X-ray Raman and small-angle X-ray scattering techniques, Nilsson et al., explored the water structure in the hydration shells of cations.[4] Nielson et al. studied the $Li^+$ hydration in concentrated aqueous solutions using neutron diffraction experiments.[5] Several ab initio molecular dynamics studies are performed by Laaksonen et al.,[6] Rempe et al.,[7,8] and Roux et al.[9] to understand the hydration structure of water around alkali cations. Marcus et al. provided extensive experimental thermodynamic data related to ion solvation.[10−13] Leung et al.[14] used thermodynamic integration and ab initio molecular dynamics (MD) simulations to determine the solvation free energies of $Li^+$ and $Cl^-$. Pratt and coworkers introduced the quasichemical theory (QCT) to understand the thermodynamics of ion solvation.[15,16] Beck and coworkers used polarizable models and QCT to investigate the thermodynamics and hydration structure around aqueous ions.[17]

Much less information is available on the dynamics of ion solvation, particularly the kinetics and mechanism of solvent-exchange process. The reactivity of ions in solutions requires rearrangement of the hydration shell,[18,19] which involves replacement of a solvent molecule from the first coordination shell. This process, also known a solvent-exchange reaction, can be represented by the following formula.

$$[I^z(H_2O)] + H_2O^* \rightleftharpoons [I^z(H_2O)_{n-1}(H_2O^*)] + H_2O$$

Here, "I" represents the ion carrying charge "$z$", "$n$" represents the number of solvent molecules in the first coordination shell around the ion, and "$H_2O^*$" represents the incoming solvent molecule.

From the reaction, it can be seen that the reactants and products are identical, and also, the incoming and outgoing solvent molecules are similar, which makes it difficult to determine solvent-exchange rates and mechanisms through experiments. Computer simulations such as MD simulations could provide more molecular-level insight. Only a few experimental techniques such as nuclear magnetic resonance (NMR) spectroscopy,[20−22] quasi-elastic neutron scattering spectroscopy,[23,24] and ligand substitution studies are employed to determine solvent-exchange rates,[25] with NMR spectroscopy being the most commonly used technique. Various methods

**Received:** March 24, 2014
**Revised:** May 21, 2014





dx.doi.org/10.1021/jp502922c | J. Phys. Chem. B XXXX, XXX, XXX−XXX

used with NMR include relaxation time measurements, line shape analysis, and isotopic labeling.[26,27]

Mechanistic classification of the solvent-exchange process is similar to the classification of ligand substitution reactions proposed by Langford and Gray.[28] According to Langford and Gray, ligand substitution reactions are categorized in three groups: (1) associative, (2) dissociative, and (3) interchange. In an associative mechanism, an intermediate with an increase in coordination number is detected. In a dissociative mechanism, an intermediate with a decrease in coordination number is detected. In an interchange mechanism, no kinetically detectable intermediate is created, which means the incoming and outgoing ligands exchange almost at the same time. These mechanisms also are similar to substitution reactions in organic chemistry. The associative mechanism is similar to $S_N2$, while the dissociate mechanism is similar to $S_N1$. The key parameter that determines which mechanism for the solvent-exchange reaction should be assigned is the activation volume ($\Delta V^{\ddagger}$).[29,30] $\Delta V^{\ddagger}$, which is the difference between the partial molar volume of the reactants and the transition state, can be determined from the pressure dependence of the rate constants. Activation volumes from experiments are determined using pressure-dependent NMR studies.

The mechanism and rates for water exchange greatly depend on the type of ion involved and the charge it carries. Previous studies found that the lifetimes of water molecules in the first hydration shell vary from $10^{-10}$ s to $10^{10}$ s, depending on the nature of the ion.[29,30] Computer simulations can provide valuable molecular-level insight into understanding these variations.

Previously, several computational studies of the solvent-exchange process focused on the residence times of water molecules in the first hydration shell from equilibrium solvation, but little attention has been given to the mechanistic process.[31−35] Moreover, determining the residence times of slow solvent-exchange processes, which are in the range of nanoseconds, is not feasible with such methods.

Two techniques are mainly used for studying the mechanism of solvent-exchange reactions: quantum chemical methods and MD methods. In quantum chemical methods, quantum chemical calculations are performed on clusters of reactants, transition states, and intermediates. Aakesson et al.[36,37] and Rotzinger et al.[38−41] performed several quantum calculations using *penta*, *hexa*, and *hepta* hydrates of 3d ions to understand the solvent-exchange mechanism occurring around these ions. Exchange mechanisms were determined from the activation energies and bond lengths or alternatively computing $\Delta V^{\ddagger}$ through changes in volumes from the ground state to the excited state using Connolly surfaces.[42,43] However, these methods do not include the solvent molecules beyond the first solvation shell, and it is hard to estimate the exchange mechanism from the quantum calculation on isolated clusters. Hynes et al.[44−48] and Hermansson et al.[46,49,50] are pioneers in the use of MD methods to study the solvent-exchange process. They used the reaction rate theory to study the solvent-exchange process around aqueous $Li^+$ and $Na^+$ ions using classical nonpolarizable force fields.[45,46] This approach is similar to the one used to study the interconversion reaction between solvent separated and contact ion pairs. Later, Rustad and Stack[51] performed pressure-dependent studies on the solvent-exchange process of the aqueous $Li^+$ ion and determined the activation volume. Kerisit and Rosso[52] studied water-exchange rates around $Na^+$ and $Fe^{2+}$. To date, the majority of solvent-exchange studies have focused on cations,[29,30,53−56] and much less is known about the solvent-exchange process around aqueous anions.

In this article, we summarize our recent solvent-exchange studies around various ions. Our studies differ from previous studies in that we incorporate polarization effects in the potential models. We also perform comparative studies using various rate theories. The primary focus of our work is to develop molecular models that describe the thermodynamics and kinetics of the water-exchange process around aqueous ions. The rest of the article is organized as follows. In Simulations and Methods, we present a brief description of the methods that were employed to calculate the rate constants. In Water Exchange in Pure Water, we discuss the solvent-exchange process in pure water. In Water Exchange around Aqueous Li+, we present a discussion of solvent exchange around the aqueous $Li^+$ ion. In Water Exchange in Aqueous Halide Ions, we discuss water exchange around halide ions (chloride, bromide, and iodide). In Pressure-Dependent Rate Studies on Na+−Cl− Ion-Pair Dissociation in Water, we present our pressure-dependent studies on the ion pair interconversion for the $Na^+-Cl^-$ pair in water.

## 2. SIMULATIONS AND METHODS

**2.1. Potential of Mean Force.** The methods used in our study are very similar to those implemented by Hynes and coworkers.[44−48] To compute the rate constants, a potential of mean force (PMF) along a particular reaction coordinate is needed. Here, the reaction coordinate is defined as the center of mass separation between the ion and a chosen water molecule. PMFs are computed using eq 1.

$$W(r) = -\int_{r_0}^{r} F(r)\, \mathrm{d}r \tag{1}$$

In eq 2, $\vec{F}_1$ and $\vec{F}_2$ are the forces acting on the ion and the chosen water molecule. The term $\vec{r}_{com}$ is the unit vector along the center of mass separation between the ion and the water molecule, and $\langle ... \rangle$ represents the average over several configurations.

$$F(r) = \frac{1}{2}\langle \vec{r}_{com} \cdot (\vec{F}_2 - \vec{F}_1) \rangle \tag{2}$$

**2.2. Rate Constants.** Using the PMFs obtained from eq 1, we compute the transition state theory (TST) rate constants using eq 3.[57−60] Here $r^*$ is the position of the barrier top, and $\mu$ is the ion−water or ion−ion reduced mass.

$$k^{TST} = \sqrt{\frac{k_b T}{2\pi\mu}} \frac{(r^*)^2 \exp\left(\frac{W(r^*)}{k_b T}\right)}{\int_0^{r^*} r^2 \exp\left(\frac{W(r)}{k_b T}\right) \mathrm{d}r} \tag{3}$$

It is well-known that TST significantly overestimates the values of rate constants because it assumes once the reactive species reaches the transition state they are on the products side of the reaction. The actual rate constant accounting for recrossings resulting from the solvent dynamics is given by $k = \kappa k^{TST}$, where $\kappa$ is the transmission coefficient, which gives the probability of successful exchanges at the transition state. We computed the transmission coefficients using two different methods: Grote−Hynes (GH) theory and the reactive flux (RF) method.


dx.doi.org/10.1021/jp502922c | J. Phys. Chem. B XXXX, XXX, XXX−XXX

In accordance with GH theory, the transmission coefficient $\kappa_{GH}$ is obtained by iteratively solving eq 4.[59,61,62]

$$\kappa_{GH} = \left(\kappa_{GH} + \int_0^\infty dt\ \frac{\zeta(t)}{\omega_b} e^{-\omega_b \kappa_{GH} t}\right)^{-1} \tag{4}$$

In this equation, $\zeta(t)$ is the time-dependent friction kernel acting on the reaction coordinate, and $\omega_b$ is the barrier frequency determined through parabolic approximation to the PMF at the barrier region. The time-dependent friction kernels $\zeta(t)$ acting on the reaction coordinate at $r^*$, is computed using eqs 5 and 6.

$$\zeta(t) = \frac{1}{\mu k_b T}\langle R(t, r^*) \times R(0, r^*)\rangle \tag{5}$$

$$R(t, r) = F(t, r^*) - \langle F(t, r)\rangle \tag{6}$$

In accordance with the RF method, the transmission coefficient, $\kappa_{RF}$, is determined from the plateau value of the time-dependent transmission, $\kappa(t)$, given by eq 7.[57,63] Here, $\dot{r}(0)$ is the initial ion−water velocity along the reaction coordinate, and $\theta(x)$ is a Heaviside step function, which is 1 when $x > 0$ and 0 otherwise.

$$\kappa(t) = \frac{\langle \dot{r}(0)\theta[r(t) - r^*]\delta(r - r^*)\rangle}{\langle \dot{r}(0)\theta[\dot{r}(0)]\delta(r - r^*)\rangle} \tag{7}$$

**2.3. Activation Volume.** The key parameter for determining the solvent-exchange mechanism is the activation volume, $\Delta V^{\ddagger}$. It is defined as $V^{\ddagger} - V^{\text{reactant}}$, which is the difference between the partial molar volume of the transition state and that of the reactants, which can be obtained from the pressure dependence of rate constants given by eq 8.

$$\Delta V^{\ddagger} = -RT\left(\frac{\partial \ln(k)}{\partial P}\right)_T \tag{8}$$

The pressure dependence of $\Delta V^{\ddagger}$ is small, and a linear approximation to eq 8 given by eq 9 is typically valid for water-exchange reactions. A negative $\Delta V^{\ddagger}$ value indicates that the solvent-exchange mechanism is associative, whereas a positive value indicates that the mechanism is dissociative.

$$\ln\left(\frac{k_p}{k_0}\right) = -\Delta V^{\ddagger}\frac{P}{RT} \tag{9}$$

**2.4. Simulation Details.** All MD simulations are performed using a modified version of the Amber 9 package.[64] Polarizable force-field parameters used for ions and water were those previously developed in our research group.[65,66] To compute PMF, a series of MD simulations are carried out at various center of mass separation distances. In each of these simulations, the center of mass separation between the ion and the chosen water molecule is fixed, and the solvent configurations are sampled to evaluate the mean force $F(r)$ using eq 2. All the MD simulations are performed using the periodic boundary conditions on all three directions with a time step of 2 fs. The long-range electrostatic interactions are handled using the Ewald summation technique.[67] The SHAKE algorithm is employed in the simulations to fix the internal geometry of water.[68] More details of simulations are provided in the previous publications from our group.[69,70]

## 3. WATER EXCHANGE IN PURE WATER

In Figure 1, we present the PMFs for a $H_2O-H_2O$ pair in aqueous solution at three different pressures. Although the free energy profiles are similar at different pressures, the decreasing trend in barrier heights with pressure is noticeable. With an increase in pressure, a slight left shift is noticed in the barrier position. The results for the water exchange are summarized in Table 1. As expected, because of the decrease in barrier heights, we notice an increasing trend in $k^{TST}$ as pressure increases. The computed activation volume is −2.1 $cm^3$/mol. As discussed earlier, the negative activation volume resulting from the increase in rate constant values as pressure increases indicates an associative mechanism for the exchange of water molecule from the first solvation shell.

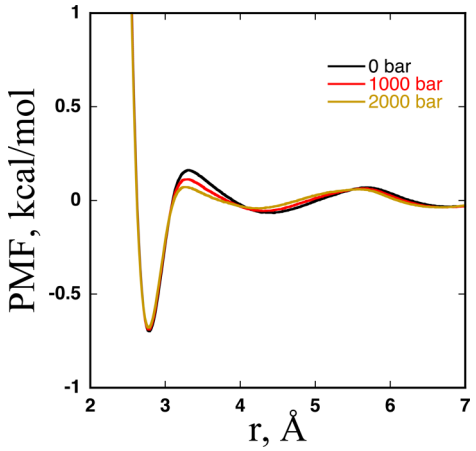


**Figure 1.** Computed PMFs for the $H_2O-H_2O$ pair at three different pressures.

In Figure 2a, we present the time-dependent transmission coefficient computed using eq 7 at various pressures. To compute $\kappa(t)$, a 10 ns simulation was carried out by constraining the reaction coordinate at the transition state. Simulation snapshots were saved every 4 ps. With the use of each of these configurations, MD simulations were run both forward and backward for 2 ps with no constraints. The initial velocities were sampled through a Boltzmann distribution. The value of $\kappa_{RF}$ was determined from averaging $\kappa(t)$ over the last 0.5 ps. The same protocol is applied for all the cases that will be discussed later in the article. The values are reported in Table 1. Transmission coefficients are very low, indicating the existence of significant recrossing events induced by the solvent dynamics. The value of $\kappa_{RF}$ slightly increases as pressure increases. The activation volume obtained from the RF-method rate constants is −6.7 $cm^3$/mol.

In Figure 2b, we present the time-dependent friction kernels $\zeta(t)$ at different pressures computed using GH theory. The corresponding $\kappa_{GH}$ values are reported in Table 1. All friction kernels show two decay timescales. We also notice that the transmission coefficients computed from GH theory decrease as pressure increases, and also, the rate constants determined from GH theory show a decreasing trend with the pressure. This observation is opposite to the trend noticed when the RF method is used. A similar kind of opposite trend in rate constants for GH theory has been noticed previously in the solvent-exchange studies of $Li^+$.

In Table 1, we also present the residence times of water. The RF-method residence time obtained from our simulations at 0


dx.doi.org/10.1021/jp502922c | J. Phys. Chem. B XXXX, XXX, XXX−XXX

**Table 1. Rate Theory Results for Pure Water System**

| pressure (MPa) | barrier height (kcal/mol) | $k^{TST}$ ($ps^{-1}$) | $\kappa_{RF}$ | $\kappa_{GH}$ | $\tau = (\kappa_{RF}k^{TST})^{-1}$ (ps) | $\tau = (\kappa_{GH}k^{TST})^{-1}$ (ps) |
|---|---|---|---|---|---|---|
| 0 | 0.86 | 1.69 | 0.085 | 0.038 | 6.9 | 15.6 |
| 100 | 0.80 | 1.84 | 0.094 | 0.028 | 5.7 | 19.4 |
| 200 | 0.75 | 2.00 | 0.128 | 0.022 | 3.9 | 22.7 |
| $\Delta V^{\ddagger}$ ($cm^3$/mol) | | −2.1 | −6.7 | 4.6 | | |

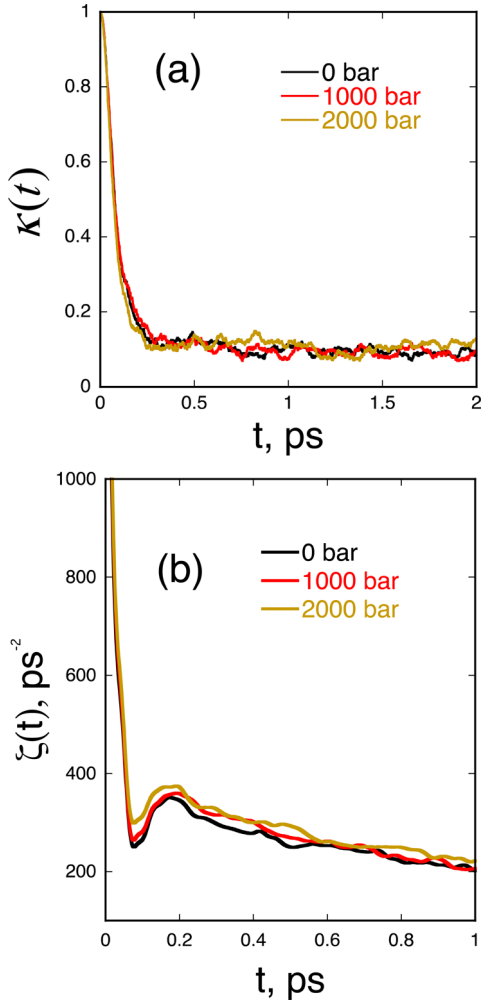


**Figure 2.** (a) Time-dependent transmission coefficients, $\kappa(t)$, of $H_2O-H_2O$ pair from RF method at three different pressures. (b) Time dependence friction kernels, $\zeta(t)$, for $H_2O-H_2O$ pair computed from GH theory at three different pressures.

MPa is 6.9 ± 1 ps. This value is close to the residence time estimated from the NMR experiments of Hertz and coworkers (~8 ps).[71] Also, Hynes and coworkers reported 4.9 ± 1 ps in their computational studies of an $H_2O-H_2O$ system.[47] The minor difference in the estimation could be due to the difference in the force fields employed.

## 4. WATER EXCHANGE AROUND AQUEOUS $LI^+$

In Figure 3, we present the PMFs for $Li^+$ at three different pressures 0, 150, and 300 MPa. All the free energy profiles are very similar. There are noticeable differences in the barrier heights. As the pressure increases, the barrier height decreases from 4.07 ± 0.05 kcal/mol at 0 MPa to 3.77 ± 0.05 kcal/mol at 300 MPa. Also, with the increase in pressure, a slight left shift is noticed in the center of mass separation distance corresponding

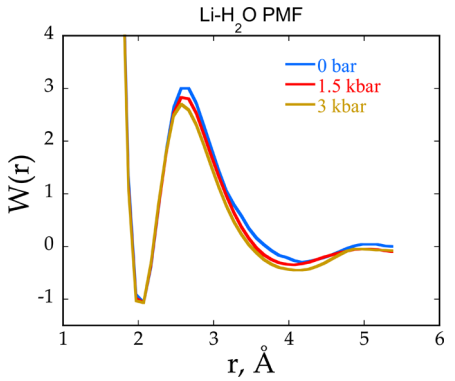


**Figure 3.** Computed PMFs for $Li^+-H_2O$ systems at three different pressures 0, 150, and 300 MPa.

to the transition state (from 2.67 to 2.57 Å). Hynes and coworkers reported 3 kcal/mol at 2.70 Å at 0 MPa pressure.[46] Barrier heights reported by Rustad and coworkers are 2.93 and 2.65 kcal/mol at 0 and 200 MPa, respectively.[51] The decreasing trend in barrier heights with pressure also was observed in the studies of Rustad and coworkers.[51] The minor differences in the barrier heights could be attributed to the difference in force fields that describe the ion−water interaction. The rate constants computed using TST are reported in Table 2. The

**Table 2. Rate Theory Results for $Li^+$ in Water**

| pressure (MPa) | barrier height (kcal/mol) | $k^{TST}$ ($ps^{-1}$) | $\kappa_{RF}$ | $\kappa_{GH}$ |
|---|---|---|---|---|
| 0 | 4.07 | $2.38 \times 10^{-2}$ | 0.22 | 0.37 |
| 150 | 3.90 | $3.14 \times 10^{-2}$ | 0.23 | 0.23 |
| 300 | 3.77 | $3.43 \times 10^{-2}$ | 0.24 | 0.02 |
| $\Delta V^{\ddagger}$ ($cm^3$/mol) | | −3.2 | −4.1 | |

computed $k^{TST}$ values increase as pressure increases, which are a direct consequence of the barrier height. In accordance with TST, the higher the barrier, the lower the rate constant. Rustad and coworkers observed the same trend in their pressure-dependence studies on $Li^+$.[51] The activation volume obtained using the TST rate constants is −3.2 $cm^3$/mol. As discussed earlier, the negative activation volume obtained from TST indicates an associative mechanism for the exchange process.

In Figure 4a, we show the time-dependent transmission coefficient, $\kappa(t)$. The computed transmission coefficients $\kappa_{RF}$ are shown in Table 2. As the pressure increases, the values of $\kappa_{RF}$ also increase, implying that pressure has considerable effect on the transmission coefficient. The activation volume computed using the rate constants from the RF method, $\kappa_{RF}k^{TST}$ is −4.1 $cm^3$/mol. This value is more negative than the activation volume obtained from TST; therefore, the pressure dependence of both the barrier height and the transmission coefficient contribute to the activation volume. The plots shown in Figure 4b correspond to the time-dependent friction kernels $\zeta(t)$ at different pressures. In all cases, there are two


dx.doi.org/10.1021/jp502922c | J. Phys. Chem. B XXXX, XXX, XXX−XXX

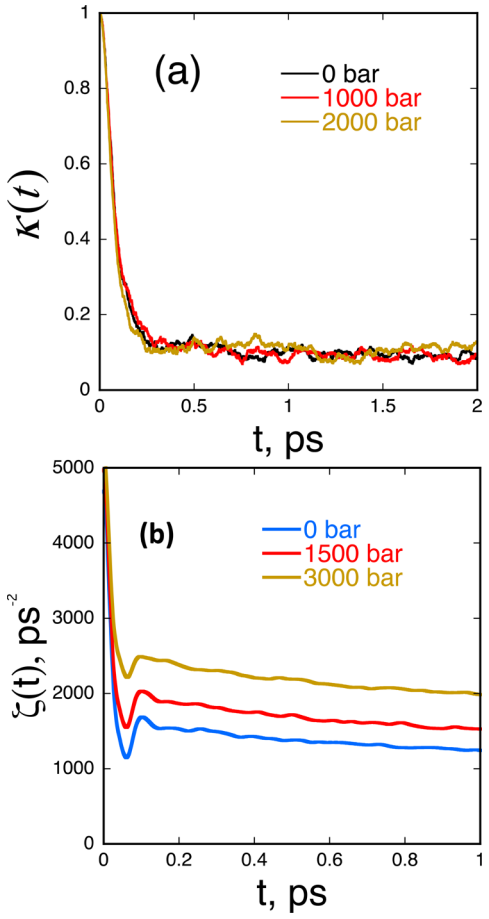


**Figure 4.** (a) Pressure dependence of the time-dependent transmission coefficients, $\kappa(t)$, of $Li^+-H_2O$ systems from the RF method. (b) Pressure dependence of the time-dependent friction kernels, $\zeta(t)$, of $Li^+-H_2O$ systems computed from GH theory.

distinct decay timescales that show initial rapid subpicosecond decay and then a longer time decay that lasts for few picoseconds. This oscillating $\zeta(t)$ reflects strong interaction between $Li^+$ and $H_2O$, which also is evident from the barrier heights of the computed PMFs. We noticed a decrease in barrier frequency with the increase in pressure. The transmission coefficients obtained from GH theory also are reported in Table 2. These values are in contrast to the actual transmission coefficients computed using the RF method. From these results, it appears that GH theory does not provide good approximation of transmission coefficients at high pressures. Spangberg and coworkers[46] also observed poor performance in their solvent-exchange studies on $Li^+$. They attributed this poor performance of GH theory to the recrossing trajectories that make large excursions from $r^*$, which violates the assumptions of GH theory.[46] Our computed residence times from RF method are 191, 140, and 120 ps at 0, 150, and 300 MPa, respectively. Our residence time value at 0 MPa compares well with the residence time reported by Rustad et al.[51]

## 5. WATER EXCHANGE IN AQUEOUS HALIDE IONS

In Figure 5, we show the pressure dependence of PMFs, W(r), for three different anions (chloride, bromide and iodide). PMFs are computed at three different pressures: 0, 100, and 200 MPa. By comparing all three plots, one observes that, as would be

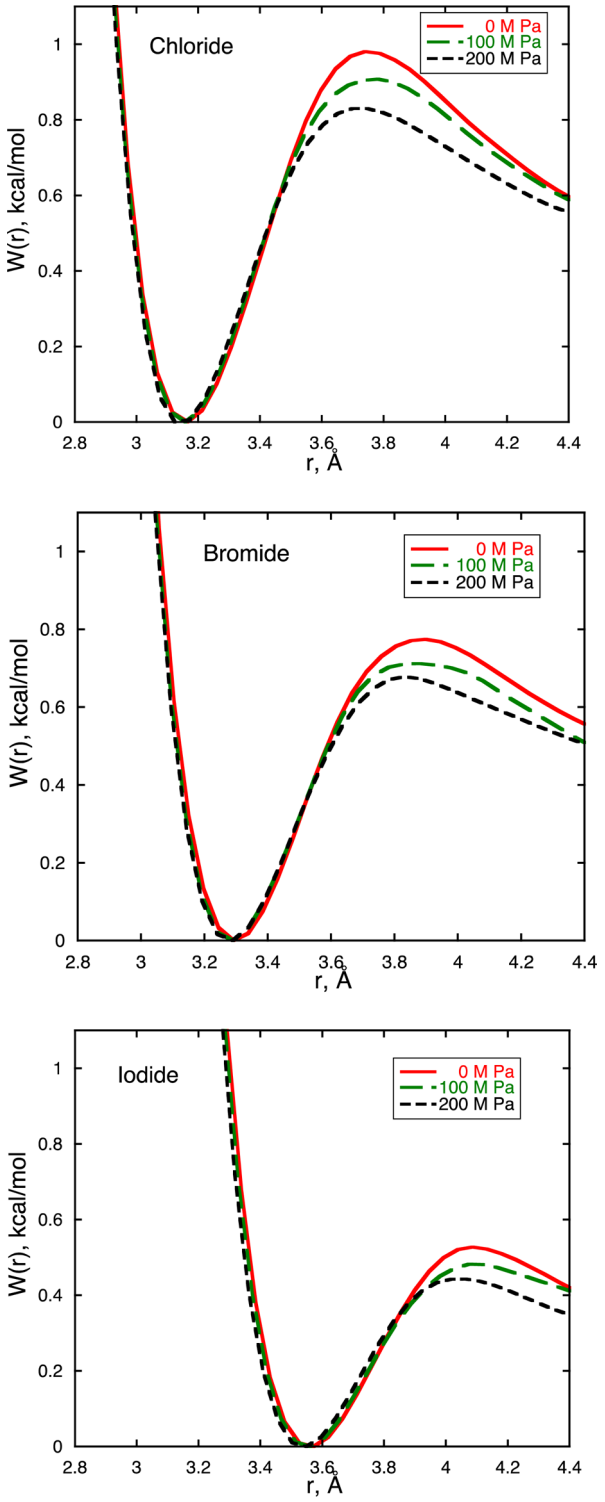


**Figure 5.** Pressure dependence of the PMFs for $Cl^--H_2O$, $Br^--H_2O$, and $I^--H_2O$ systems.

expected, barrier height decreases as ion size increases. Similar to $Li^+$, PMFs of all halide ions also exhibit a decreasing trend in barrier heights as pressure increases. The decrease in barrier height is 0.15 kcal/mol for chloride, 0.10 kcal/mol for bromide, and 0.09 kcal/mol for iodide. From these values, one observes that the pressure dependence of the barrier height is more prominent for chloride and decreases as the ion size increases. The rate constants obtained from TST are reported in Table 3.


dx.doi.org/10.1021/jp502922c | J. Phys. Chem. B XXXX, XXX, XXX−XXX

**Table 3. Rate Theory Results for Halide Ions in Water**

| | pressure (M Pa) | $k^{TST}$ ($ps^{-1}$) | $\omega_b$ ($ps^{-1}$) | $\kappa_{GH}$ | $\kappa_{RF}$ | $\tau_{RF} = (\kappa_{RF}k^{TST})^{-1}$ ps |
|---|---|---|---|---|---|---|
| | 0 | 1.07 | 13.37 | 0.043 | 0.101 | 9.2 |
| chloride | 100 | 1.20 | 12.52 | 0.027 | 0.044 | 19.1 |
| | 200 | 1.32 | 11.70 | 0.018 | 0.024 | 31.5 |
| | 0 | 1.22 | 10.80 | 0.034 | 0.085 | 9.6 |
| bromide | 100 | 1.33 | 9.96 | 0.025 | 0.053 | 14.2 |
| | 200 | 1.46 | 8.99 | 0.020 | 0.045 | 15.3 |
| | 0 | 1.52 | 10.26 | 0.035 | 0.094 | 7.0 |
| iodide | 100 | 1.64 | 9.54 | 0.028 | 0.045 | 13.6 |
| | 200 | 1.78 | 8.36 | 0.020 | 0.044 | 12.8 |

[a]The estimated error in transmission coefficients is ±0.01.

With the increase in pressure, the $k^{TST}$ increases for all the anions. The pressure dependence of $k^{TST}$ is similar in the case of $Li^+$ as well as for halides. The activation volume values obtained from TST for all the anions are presented in Table 4. The values are negative for all the anions, thus indicating an associative mechanism for all anions.

**Table 4. Activation Volumes Computed from Various Rate Theories for Halide Ions in Water**

| | transition state theory ($\Delta V^{\ddagger}$, $cm^3$/mol) | Grote−Hynes theory ($\Delta V^{\ddagger}$, $cm^3$/mol) | reactive flux method ($\Delta V^{\ddagger}$, $cm^3$/mol) |
|---|---|---|---|
| chloride | −2.7 | 8.4 | 15.8 |
| bromide | −2.2 | 4.3 | 6.5 |
| iodide | −1.9 | 4.6 | 9.3 |

[a]The estimated error in activation volumes is ±2 $cm^3$/mol

Similar to the $Li^+$ and pure water cases, we also computed the actual solvent-exchange rate constants using the RF method for all the anions. We used the same protocol described earlier to compute the time-dependent transmission coefficient $\kappa(t)$. In Figure 6, we show the computed $\kappa(t)$ for all the anions at different pressures. The computed transmission coefficients, $\kappa_{RF}$, determined using the RF method are reported in Table 3. It can be seen that $\kappa_{RF}$ decreases as pressure increases. The activation volumes computed using the rate constants from the RF method, $\kappa_{RF}k^{TST}$, are presented in Table 4. The activation volumes are positive for all the anions, indicating a dissociative mechanism. This is contrary to the TST result. The rate constants from TST increase as pressure increases, whereas the actual rate constants obtained using the RF method decrease as pressure increases for all the anion cases. This result emphasizes the importance of dynamical effects in determining the rates and mechanism of the solvent-exchange process. In Figure 7, we show the time-dependent friction kernels for all the anions at various pressures. Similar to the previous cases, all the plots show similar behaviors with two decay timescales. The computed transmission coefficients from GH theory, $\kappa_{GH}$, are shown in Table 3. Similar to the results obtained using the RF method, the transmission coefficients decrease as pressure increases. Activation volumes for all the anions obtained using GH theory reported in Table 4 are also positive, indicating a dissociative mechanism.

## 6. PRESSURE-DEPENDENT RATE STUDIES ON $NA^+$−$CL^-$ ION-PAIR DISSOCIATION IN WATER

After studying the solvent-exchange rates and mechanisms occurring around aqueous ions, we performed analogous pressure-dependent rate studies on the $Na^+$−$Cl^-$ ion-pair dissociation reaction in water. In Figure 8, we show the PMFs for $Na^+$−$Cl^-$ ion pair in water at three different pressures. PMFs are computed using the constrained mean force approach, as described previously in Simulations and Methods. Similar to the trend observed for $Li^+$ and the halides, PMFs for the $Na^+$−$Cl^-$ pair also exhibit decreasing barrier heights as pressure increases, resulting in an increase of the value of TST rate constants as the pressure increases. Rate constant values are reported in Table 5. Using TST rate constants and eq 9, we obtained an activation volume of −2.4 $cm^3$/mol.

In Figure 9a, we present the time-dependent transmission coefficient $\kappa(t)$ for a $Na^+$−$Cl^-$ pair in water at different pressures. The corresponding $\kappa_{RF}$ values are reported in Table 4. It can be seen that the transmission coefficients decrease as the pressure increases. This trend is similar to the trend observed for halides and opposite to that observed for $Li^+$. The actual rate constants from the RF method presented in Table 4 show a decreasing trend with the increasing pressure. We computed the relaxation times $\tau_{RF} = (\kappa_{RF}k^{TST})^{-1}$ using the rate constants obtained using the RF method. The results are reported in Table 5. The relaxation time for the ion-pair dissociation at 0 MPa obtained from our simulation is 22.5 ps, which is comparable to 20 ps reported by Chandler and coworkers.[72] The activation volume computed from the rate constants of the RF method is 1.58 $cm^3$/mol. By applying the same mechanistic interpretation of activation volume to the ion-pair dissociation reaction, it appears that the $Na^+$−$Cl^-$ pair in water exhibits an $S_N1$ type or dissociative mechanism according to the RF method. This means that, at the transition state, bond breaking dominates; that is, the chloride ion leaves the first solvation shell of $Na^+$, followed by a water molecule entering into the first solvation shell. For comparison, we also computed the time-dependent friction kernels shown in Figure 9b and $\kappa_{GH}$ reported in Table 5. The transmission coefficient does not change significantly with pressure. There, the rate constants obtained using GH theory, $\kappa_{GH}k^{TST}$ follow same trend as TST rate constants.

## 7. CONCLUSION AND OUTLOOK

In this article, we present a summary of our recent studies of the dynamics of the ion-solvation process. We used the rate theory approach to determine the solvent-exchange rates. Also, analogous to experimental procedures, we computed pressure-dependent rates to determine the activation volume, which is a key indicator for the solvent-exchange mechanism. We performed a systematic study using four systems: (1) a pure solvent, (2) a cation ($Li^+$), (3) anions (halides), and (4) an ion-pair ($Na^+$−$Cl^-$) dissociation process. From our results, we


dx.doi.org/10.1021/jp502922c | J. Phys. Chem. B XXXX, XXX, XXX−XXX

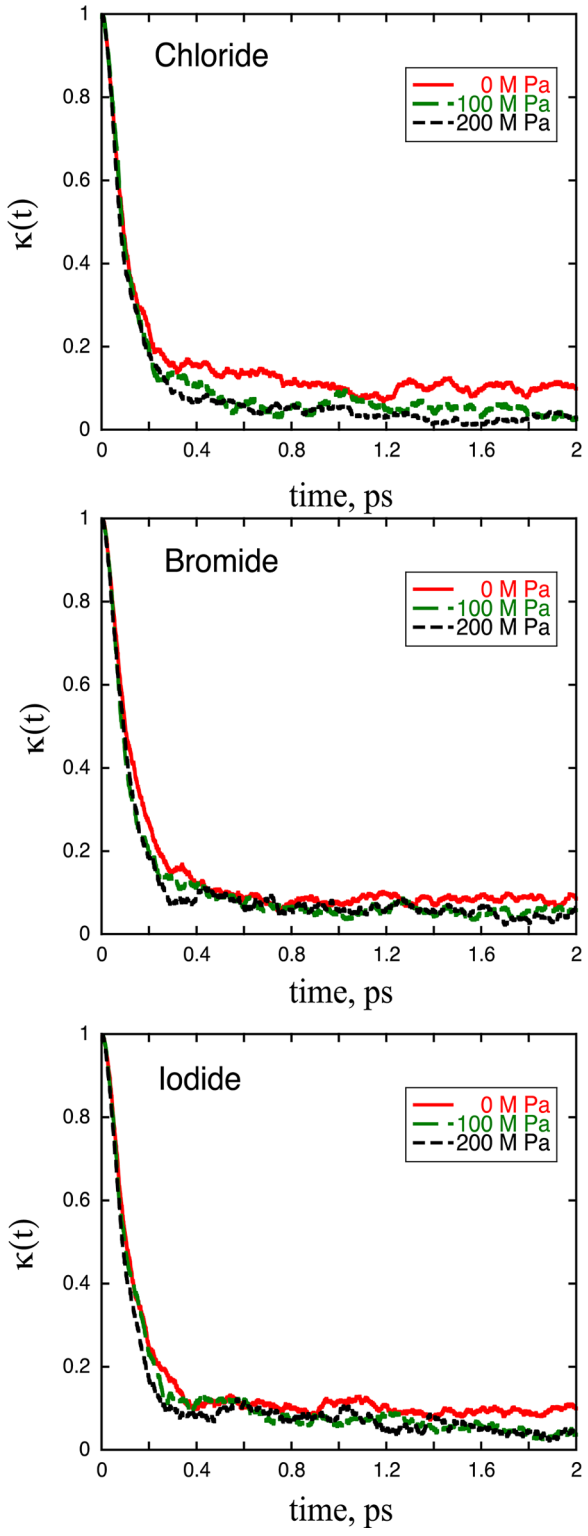


**Figure 6.** Computed time-dependent transmission coefficients, $\kappa(t)$, for $Cl^-$–$H_2O$, $Br^-$–$H_2O$, and $I^-$–$H_2O$ systems.

notice that, because of the decrease in barrier heights, TST rate constants increase as pressure increases for all the cases. Therefore, TST results for all cases give a negative activation volume, which is indicative of an associative mechanism. We also computed pressure-dependent rate constants using the RF method, which takes in to account recrossings induced by solvent dynamics.

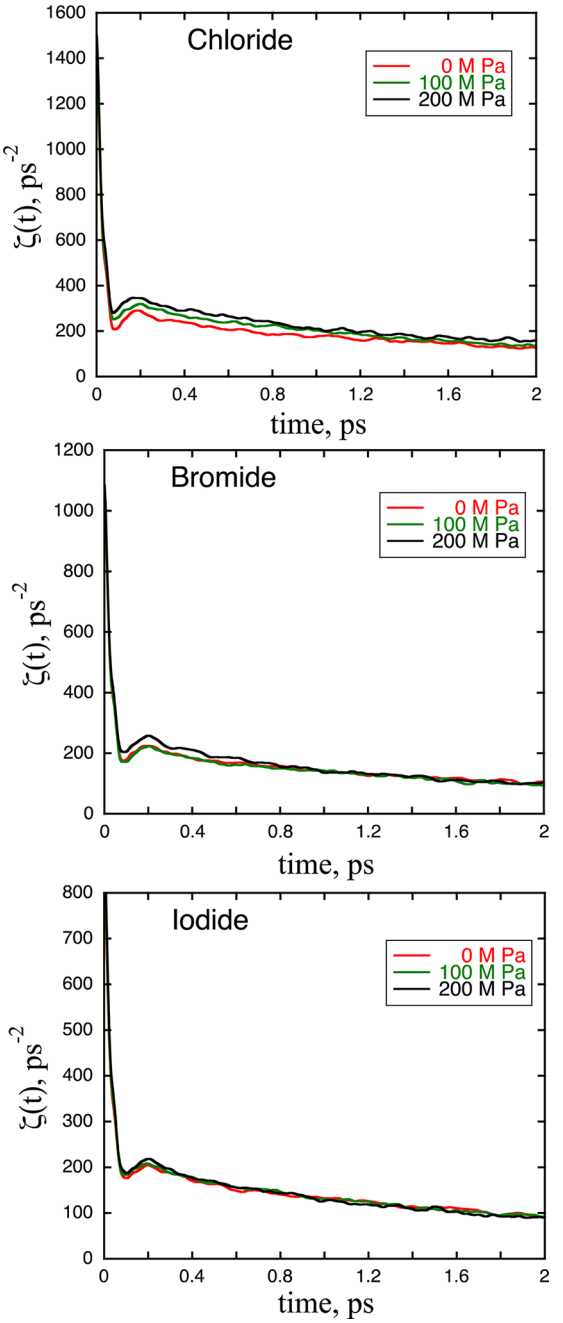


**Figure 7.** Computed time-dependent friction kernels, $\zeta(t)$, for $Cl^-$–$H_2O$, $Br^-$–$H_2O$, and $I^-$–$H_2O$ systems.

**Pure Water.** The effect of pressure on transmission coefficients obtained using the RF method for pure water follows the TST rate constants. Therefore, rate constants obtained using the RF method also increase as pressure increases, thus agreeing with the TST predicted mechanism (associative) for the exchange process.

**Aqueous $Li^+$.** The value of $\kappa_{RF}$ increases as pressure increases. Both $k^{TST}$ rate and $\kappa_{RF}$ increase with pressure, which results in a negative activation volume that is indicative of an associative mechanism for the exchange process.

**Aqueous Halides.** The value of $\kappa_{RF}$ decreases as pressure increases. Here, we notice that the $k^{TST}$ rate and $\kappa_{RF}$ have an opposite trend as pressure increases. The effect of pressure on the transmission coefficient overshadows the effect on the


dx.doi.org/10.1021/jp502922c | J. Phys. Chem. B XXXX, XXX, XXX–XXX

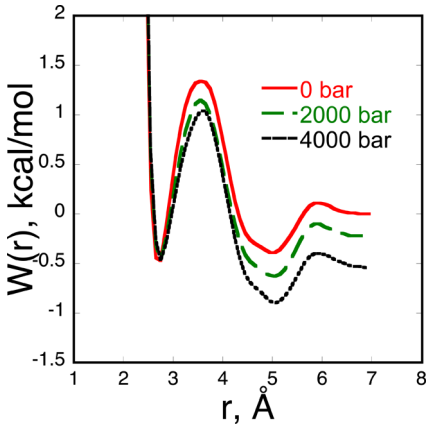


**Figure 8.** Computed PMFs for $Na^+-Cl^-$ pairs in water at different pressures.

barrier and results in a net decrease of the rate constant, $\kappa_{RF}k^{TST}$, obtained using the RF-method as pressure increases. Therefore, we obtain a positive activation volume for all the halides from the rate constants obtained using the RF method. This indicates a dissociative mechanism.

**$Na^+-Cl^-$ Ion-Pair in Water.** The value of $\kappa_{RF}$ decreases as pressure increases. The values of $k^{TST}$ and $\kappa_{RF}$ have opposite trends as pressure increases. Therefore, similar to the halides, the effect of pressure on the transmission coefficient overshadows the effect on the barrier height and results in a net decrease of the rate constant obtained using the RF method as pressure increases and gives a positive activation volume. If one applies the same mechanistic interpretation of activation volumes similar to solvent-exchange mechanisms, our results obtained using the RF method indicates a dissociative mechanism for the $Na^+-Cl^-$ ion-pair dissociation reaction in water.

The polarizable models employed in the current studies yield different barrier heights and transmission coefficients compared to previous studies of nonpolarizable models, and it has not been established that polarizable models are better. Also, our rate theory results do not take into account the nuclear quantum effect (NQE), which plays an important role in hydrogen-bonded systems. In the past, we performed path integral Monte Carlo simulations on the chloride/iodide $(H_2O)_n$ clusters to determine the importance of NQE on structures and to explore the quantum effects of nuclei of the clusters in the processes of hydrogen bond rearrangement.[73,74] It was found that, because of the quantum delocalization of nuclei, especially hydrogen, the calculated quantum radial distribution functions are less structured and slightly shifted outward compared to the corresponding classical description. The NQE also contributed significantly to the binding enthalpy of the clusters at lower temperatures. Path-integral techniques have also been used to investigate a variety of interesting problems. For instance, studies have been performed of

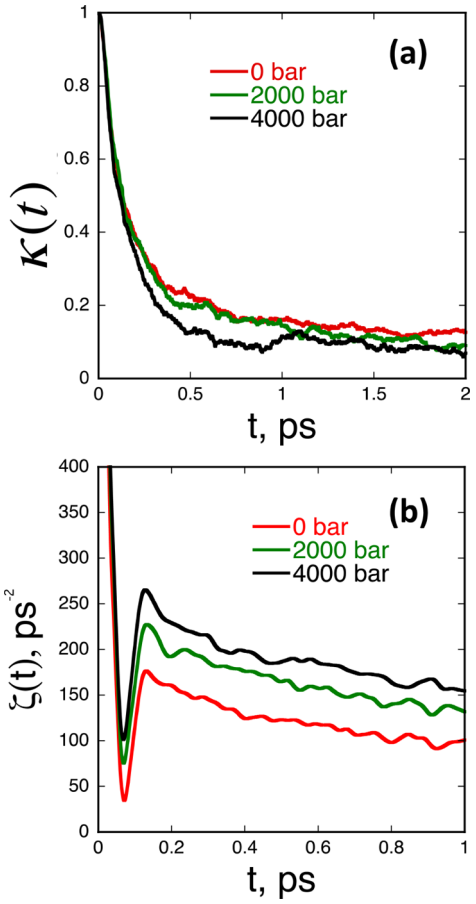


**Figure 9.** (a) Time-dependent transmission coefficients, $\kappa(t)$, of $Na^+-Cl^-$ systems from RF method at three different pressures. (b) Time-dependence friction kernels, $\zeta(t)$, of $Na^+-Cl^-$ systems computed from GH theory at three different pressures.

quantum effects on the structure of liquid water. The NQE on the hydration structure of solvated excess protons in water such as tunneling, zero-point motion, and transmission coefficients were found to be significant at finite temperatures. The NQE on the heat capacity of water have also been study using path integral method.[75−77] Ongoing research efforts in our group are focused on understanding the influence of NQEs on the dynamics of ion solvation such as the water-exchange rate and the corresponding transmission coefficients using ring polymer molecular dynamics (RPMD) simulations.[78]

We currently are focusing on similar studies at interfaces using the same set of polarizable potential models. Because of their ability to respond to the local, nonhomogeneous environment, one can expect a different response.

As discussed in the Introduction to this paper, Rempe and coworkers, Beck and coworkers, Pratt and coworkers, and Laaksonen and coworkers have made pioneering contributions through ab initio MD studies toward understanding the

**Table 5. Pressure-Dependent Rate Theory Results for $Na^+-Cl^-$ in Water**

| pressure (MPa) | barrier height (kcal/mol) | $k^{TST}$ ($ps^{-1}$) | $\kappa_{RF}$ | $\kappa_{GH}$ | $\tau = (\kappa_{RF}k^{TST})^{-1}$ ps | $\tau = (\kappa_{GH}k^{TST})^{-1}$ ps |
|---|---|---|---|---|---|---|
| 0 | 1.81 | 0.35 | 0.13 | 0.17 | 22.5 | 16.8 |
| 200 | 1.62 | 0.45 | 0.09 | 0.16 | 24.7 | 13.9 |
| 400 | 1.51 | 0.50 | 0.07 | 0.15 | 28.9 | 11.7 |
| $\Delta V^{\ddagger}$ ($cm^3$/mol) | | −2.41 | 1.59 | | | |


dx.doi.org/10.1021/jp502922c | J. Phys. Chem. B XXXX, XXX, XXX−XXX

structure and thermodynamic properties of ion hydration. However, there are no ab initio MD studies focused on the kinetics and mechanism of the solvent-exchange process. To compute solvent-exchange rates taking into account recrossing events (i.e., using the RF method), a large number of simulations would be needed, which is a challenging task with ab initio MD studies as they are computationally very expensive. However, solvent-exchange rates can be determined using residence times computed by Impey's method.[32] We are hoping to carry out these studies in the near future and will compare the results obtained with results from classical force-field models.

Also, it would be worth investigating how local charges/dipoles change in ion-solvation shells to determine the origin of differences observed when polarizable and nonpolarizable models are used.[79−81] Here, for the ion-pair case, we used a simple and analogous mechanistic interpretation that has been applied for the solvent-exchange process. However, Geissler et al.,[72] Ballard et al.,[82] and Peters et al.[83,84] have explained the complicated kinetic pathways for ion-pair dissociation.

## AUTHOR INFORMATION


### Corresponding Author

*E-mail: liem.dang@pnnl.gov.


### Notes

The authors declare no competing financial interest.

### Biographies

**Dr. Harsha V. R. Annapureddy** is currently a Postdoctoral Research Associate at Pacific Northwest National Laboratory (PNNL) since 2011. He received his Bachelor of Technology degree in Pharmaceutical Sciences and Technology from Institute of Chemical Technology (ICT), Mumbai, India. He earned his Ph.D. in chemistry from The University of Iowa in 2011. His thesis work was on computational studies of structure and dynamics of room temperature of ionic liquids. His research interests are to understand molecular interactions in complex multispecies, multiphase systems.

**Dr. Liem X. Dang** is a Scientist in the Physical Chemistry Division at the Pacific Northwest National Laboratory (PNNL), where he has been since 1991. He received his B.S. from Florida Institute of Technology in 1980 and Ph.D. from the University of California, Irvine, in 1985. He was a postdoctoral fellow at the University of California, San Francisco, and Visiting Scientist at the IBM Almaden Research Center, CA, before joining the staff at PNNL in 1991. Presently, he is also an Adjunct Professor at The School of Chemical Engineering, University of Queensland, Australia and at the Department of Metallurgical Engineering, College of Mines and Earth Sciences, University of Utah, Salt Lake City, UT. Among his honors, he is a Fellow of the American Physical Society and of the American Association for the Advancement of Science and is also on the Editorial board for the journal of Physical Chemistry A, B, C, and Letters.

## ACKNOWLEDGMENTS

The Division of Chemical Sciences, Geosciences, and Biosciences, Office of Basic Energy Sciences (BES), of the U.S. Department of Energy (DOE) funded this work. Battelle operates Pacific Northwest National Laboratory for DOE. The calculations were carried out using computer resources provided by BES.

## REFERENCES


(1) Ohtaki, H.; Radnai, T. Structure and Dynamics of Hydrated Ions. *Chem. Rev.* **1993**, *93* (3), 1157−1204.

(2) Soper, A. K.; Weckstrom, K. Ion Solvation and Water Structure in Potassium Halide Aqueous Solutions. *Biophys. Chem.* **2006**, *124* (3), 180−191.

(3) Botti, A.; Bruni, F.; Imberti, S.; Ricci, M. A.; Soper, A. K. Solvation of Hydroxyl Ions in Water. *J. Chem. Phys.* **2003**, *119* (10), 5001−5004.

(4) Waluyo, I.; Huang, C. C.; Nordlund, D.; Bergmann, U.; Weiss, T. M.; Pettersson, L. G. M.; Nilsson, A. The Structure of Water in the Hydration Shell of Cations from X-Ray Raman and Small Angle X-Ray Scattering Measurements. *J. Chem. Phys.* **2011**, *134* (6), 10753.

(5) Howell, I.; Neilson, G. W. $Li^+$ Hydration in Concentrated Aqueous Solution. *J. Phys.: Condens. Mater.* **1996**, *8* (25), 4455−4463.

(6) Lyubartsev, A. P.; Laasonen, K.; Laaksonen, A. Hydration of $Li^+$ Ion. An *ab initio* Molecular Dynamics Simulation. *J. Chem. Phys.* **2001**, *114* (7), 3120−3126.

(7) Varma, S.; Rempe, S. B. Coordination Numbers of Alkali Metal Ions in Aqueous Solutions. *Biophys. Chem.* **2006**, *124* (3), 192−199.

(8) Rempe, S. B.; Pratt, L. R.; Hummer, G.; Kress, J. D.; Martin, R. L.; Redondo, A. The Hydration Number of Li(+) in Liquid Water. *J. Am. Chem. Soc.* **2000**, *122* (5), 966−967.

(9) Rowley, C. N.; Roux, B. The Solvation Structure of $Na^+$ and $K^+$ in Liquid Water Determined from High Level *ab initio* Molecular

Dynamics Simulations. *J. Chem. Theory Comput.* **2012**, *8* (10), 3526−3535.
(10) Marcus, Y. Thermodynamics of Solvation of Ions 0.6. The Standard Partial Molar Volumes of Aqueous Ions at 298.15 K. *J. Chem. Soc., Faraday Trans. 1* **1993**, *89* (4), 713−718.
(11) Marcus, Y. Thermodynamics of Solvation of Ions 0.5. Gibbs Free-Energy of Hydration at 298.15 K. *J. Chem. Soc., Faraday Trans. 1* **1991**, *87* (18), 2995−2999.
(12) Marcus, Y. The Thermodynamics of Solvation of Ions 0.4. Application of the Tetraphenylarsonium Tetraphenylborate (Tatb) Extrathermodynamic Assumption to the Hydration of Ions and to Properties of Hydrated Ions. *J. Chem. Soc., Faraday Trans. 1* **1987**, *83*, 2985−2992.
(13) Marcus, Y. The Thermodynamics of Solvation of Ions 0.2. The Enthalpy of Hydration at 298.15 K. *J. Chem. Soc., Faraday Trans. 1* **1987**, *83*, 339−349.
(14) Leung, K.; Rempe, S. B.; von Lilienfeld, O. A. *Ab initio* Molecular Dynamics Calculations of Ion Hydration Free Energies. *J. Chem. Phys.* **2009**, *130* (20).
(15) Rogers, D. M.; Jiao, D.; Pratt, L. R.; Rempe, S. B. Chapter Four: Structural Models and Molecular Thermodynamics of Hydration of Ions and Small Molecules. In *Annual Reports in Computational Chemistry*; Ralph, A. W., Ed.; Elsevier: Amsterdam, 2012; Vol. *8*, pp 71−127.
(16) Asthagiri, D.; Pratt, L. R.; Ashbaugh, H. S. Absolute Hydration Free Energies of Ions, Ion-Water Clusters, and Quasichemical Theory. *J. Chem. Phys.* **2003**, *119* (5), 2702−2708.
(17) Rogers, D. M.; Beck, T. L. Quasichemical and Structural Analysis of Polarizable Anion Hydration. *J. Chem. Phys.* **2010**, *132* (1), 014505.
(18) Ando, K.; Hynes, J. T. HCl Acid Ionization in Water: A Theoretical Molecular Modeling. *J. Mol. Liq.* **1995**, *64* (1−2), 25−37.
(19) Ando, K.; Hynes, J. T. HF Acid Ionization in Water: The First Step. *Faraday Discuss.* **1995**, *102*, 435−441.
(20) Hrovat, M. I.; Wade, C. G. NMR Pulsed Gradient Diffusion Measurements 0.2. Residual Gradients and Lineshape Distortions. *J. Magn. Reson.* **1981**, *45* (1), 67−80.
(21) Hrovat, M. I.; Wade, C. G. NMR Pulsed-Gradient Diffusion Measurements 0.1. Spin-Echo Stability and Gradient Calibration. *J. Magn. Reson.* **1981**, *44* (1), 62−75.
(22) van Eldik, R. *Studies in Inorganic Chemistry 7: Inorganic High Pressure Chemistry, Kinetics and Measurements*; Elsevier: Amsterdam, 1986.
(23) Salmon, P. S.; Howells, W. S.; Mills, R. The Dynamics of Water-Molecules in Ionic Solution 0.2. Quasi-Elastic Neutron-Scattering and Tracer Diffusion Studies of the Proton and Ion Dynamics in Concentrated $Ni^{2+}$, $Cu^{2+}$ and $Nd^{3+}$ Aqueous-Solutions. *J. Phys. C: Solid State Phys.* **1987**, *20* (34), 5727−5747.
(24) Teixeira, J.; Bellissentfunel, M. C.; Chen, S. H.; Dianoux, A. J. Experimental-Determination of the Nature of Diffusive Motions of Water-Molecules at Low-Temperatures. *Phys. Rev. A* **1985**, *31* (3), 1913−1917.
(25) Gilligan, T. J.; Atkinson, G. Ultrasonic-Absorption in Aqueous Alkali-Metal Sulfate-Solutions. *J. Phys. Chem.* **1980**, *84* (2), 208−213.
(26) Sandstrom, J. *Dynamic NMR Spectroscopy*; Academic Press: London, 1983.
(27) Helm, L.; Nicolle, G. M.; Merbach, A. E. Water and Proton Exchange Processes on Metalions. *Advances in Inorganic Chemistry: Including Bioinorganic Studies* **2005**, *57*, 327−379.
(28) Langford, C. H. G. *Ligand Substitution Processes*; W. A. Benjamin, Inc.: New York, 1965.
(29) Helm, L.; Merbach, A. E. Inorganic and Bioinorganic Solvent Exchange Mechanisms. *Chem. Rev.* **2005**, *105* (6), 1923−1959.
(30) Helm, L.; Merbach, A. E. Water Exchange on Metal Ions: Experiments and Simulations. *Coord. Chem. Rev.* **1999**, *187*, 151−181.
(31) Bopp, P. A. In *Aqueous Ionic Solutions*, Bellissent-Funel, M.-C.; Neilson, G.W., Eds.; Reidel: Dordrechl, 1987; NATO AS1 Vol. *C205*, p 359 and references cited therein.
(32) Impey, R. W.; Madden, P. A.; McDonald, I. R. Hydration and Mobility of Ions in Solution. *J. Phys. Chem.* **1983**, *87* (25), 5071−5083.
(33) Koneshan, S.; Rasaiah, J. C.; Lynden-Bell, R. M.; Lee, S. H. Solvent Structure, Dynamics, and Ion Mobility in Aqueous Solutions at 25 °C. *J. Phys. Chem. B* **1998**, *102* (21), 4193−4204.
(34) Lee, S. H.; Rasaiah, J. C. Molecular-Dynamics Simulation of Ionic Mobility 0.1. Alkali-Metal Cations in Water at 25 °C. *J. Chem. Phys.* **1994**, *101* (8), 6964−6974.
(35) Lee, S. H.; Rasaiah, J. C. Molecular Dynamics Simulation of Ion Mobility 0.2. Alkali Metal and Halide Ions using the SPC/E Model for Water at 25 °C. *J. Phys. Chem.* **1996**, *100* (4), 1420−1425.
(36) Akesson, R.; Pettersson, L. G. M.; Sandstrom, M.; Wahlgren, U. Theoretical-Study on Water-Exchange Reactions of the Divalent and Trivalent Metal Ions of the First Transition Period. *J. Am. Chem. Soc.* **1994**, *116* (19), 8705−8713.
(37) Akesson, R.; Pettersson, L. G. M.; Sandstrom, M.; Siegbahn, P. E. M.; Wahlgren, U. Theoretical *ab initio* Scf Study of Binding-Energies and Ligand-Field Effects for the Hexahydrated Divalent Ions of the 1st-Row Transition-Metals. *J. Phys. Chem.* **1992**, *96* (26), 10773−10779.
(38) Rotzinger, F. P. Treatment of Substitution and Rearrangement Mechanisms of Transition Metal Complexes with Quantum Chemical Methods. *Chem. Rev.* **2005**, *105* (6), 2003−2037.
(39) Rotzinger, F. P. Water-Exchange Reaction of the Hexaaqua Ions of Vanadium(II), Manganese(II), and Iron(II) Revisited: A Discussion of Models with the Solvent Treated as a Dielectric Continuum. *Helv. Chim. Acta* **2000**, *83* (11), 3006−3020.
(40) Rotzinger, F. P. Mechanism of Water Exchange for the Di and Trivalent Metal Hexaaqua Ions of the First Transition Series. *J. Am. Chem. Soc.* **1997**, *119* (22), 5230−5238.
(41) Rotzinger, F. P. Structure of the Transition States and Intermediates Formed in the Water-Exchange of Metal Hexaaqua Ions of the First Transition Series. *J. Am. Chem. Soc.* **1996**, *118* (28), 6760−6766.
(42) Kowall, T.; Caravan, P.; Bourgeois, H.; Helm, L.; Rotzinger, F. P.; Merbach, A. E. Interpretation of Activation Volumes for Water Exchange Reactions Revisited: *Ab initio* Calculations for $Al^{3+}$, $Ga^{3+}$, and $In^{3+}$, and New Experimental Data. *J. Am. Chem. Soc.* **1998**, *120* (26), 6569−6577.
(43) De Vito, D.; Weber, J.; Merbach, A. E. Calculated Volume and Energy Profiles for Water Exchange on T(2g)(6) Rhodium(III) and Iidium(III) Hexaaqualons: Conclusive Evidence for an $I_a$ Mechanism. *Inorg. Chem.* **2004**, *43* (3), 858−864.
(44) Rey, R.; Hynes, J. T. Hydration Shell Exchange Dynamics for $Na^+$ in Water. *J. Phys.: Condens. Matter* **1996**, *8* (47), 9411−9416.
(45) Rey, R.; Hynes, J. T. Hydration Shell Exchange Kinetics: An MD Study for $Na^+$(aq). *J. Phys. Chem.* **1996**, *100* (14), 5611−5615.
(46) Spangberg, D.; Rey, R.; Hynes, J. T.; Hermansson, K. Rate and Mechanisms for Water Exchange around $Li^+$(aq) from MD Simulations. *J. Phys. Chem. B* **2003**, *107* (18), 4470−4477.
(47) Laage, D.; Hynes, J. T. On the Residence Time for Water in a Solute Hydration Shell: Application to Aqueous Halide Solutions. *J. Phys. Chem. B* **2008**, *112* (26), 7697−7701.
(48) Moller, K. B.; Rey, R.; Masia, M.; Hynes, J. T. On the Coupling between Molecular Diffusion and Solvation Shell Exchange. *J. Chem. Phys.* **2005**, *122* (11).
(49) Hermansson, K.; Wojcik, M. Water Exchange around $Li^+$ and $Na^+$ in LiCl(aq) and NaCl(aq) from MD Simulations. *J. Phys. Chem. B* **1998**, *102* (31), 6089−6097.
(50) Spangberg, D.; Wojcik, M.; Hermansson, K. Pressure Dependence and Activation Volume for the Water Exchange Mechanism in NaCl(aq) from MD Simulations. *Chem. Phys. Lett.* **1997**, *276* (1−2), 114−121.
(51) Rustad, J. R.; Stack, A. G. Molecular Dynamics Calculation of the Activation Volume for Water Exchange on $Li^+$. *J. Am. Chem. Soc.* **2006**, *128* (46), 14778−14779.
(52) Kerisit, S.; Rosso, K. M. Transition Path Sampling of Water Exchange Rates and Mechanisms around Aqueous Ions. *J. Chem. Phys.* **2009**, *131* (11), 114512.

(53) Buchner, R.; Capewell, S. G.; Hefter, G.; May, P. M. Ion-Pair and Solvent Relaxation Processes in Aqueous $Na_2SO_4$ Solutions. *J. Phys. Chem. B* **1999**, *103* (7), 1185−1192.
(54) Buchner, R.; Chen, T.; Hefter, G. Complexity in "Simple" Electrolyte Solutions: Ion Pairing in $Mg_2SO_4$(aq). *J. Phys. Chem. B* **2004**, *108* (7), 2365−2375.
(55) Callahan, K. M.; Casillas-Ituarte, N. N.; Roeselova, M.; Allen, H. C.; Tobias, D. J. Solvation of Magnesium Dication: Molecular Dynamics Simulation and Vibrational Spectroscopic Study of Magnesium Chloride in Aqueous Solutions. *J. Phys. Chem. A* **2010**, *114* (15), 5141−5148.
(56) Bleuzen, A.; Pittet, P. A.; Helm, L.; Merbach, A. E. Water Exchange on Magnesium(II) in Aqueous Solution: A Variable Temperature and Pressure $O^{17}$ NMR Study. *Magn. Reson. Chem.* **1997**, *35* (11), 765−773.
(57) Rey, R.; Guardia, E. Dynamic Aspects of the $Na^+$-$Cl^-$ Ion-Pair Association in Water. *J. Phys. Chem.* **1992**, *96* (11), 4712−4718.
(58) Guardia, E.; Rey, R.; Padro, J. A. Potential of Mean Force by Constrained Molecular-Dynamics: A Sodium-Chloride Ion-Pair in Water. *Chem. Phys.* **1991**, *155* (2), 187−195.
(59) Hynes, J. T. Chemical-Reaction Dynamics in Solution. *Annu. Rev. Phys. Chem.* **1985**, *36*, 573−597.
(60) Das, A. K.; Madhusoodanan, M.; Tembe, B. L. Dynamics of $Na^+$−$Cl^-$, $Na^+$−$Na^+$, and $Cl^-$−$Cl^-$ Ion Pairs in Dimethyl Sulfoxide: Friction Kernels and Transmission Coefficients. *J. Phys. Chem. A* **1997**, *101* (15), 2862−2872.
(61) Ciccotti, G.; Ferrario, M.; Hynes, J. T.; Kapral, R. Dynamics of Ion-Pair Interconversion in a Polar-Solvent. *J. Chem. Phys.* **1990**, *93* (10), 7137−7147.
(62) Zichi, D. A.; Hynes, J. T. A Dynamical Theory of Unimolecular Ionic Dissociation Reactions in Polar-Solvents. *J. Chem. Phys.* **1988**, *88* (4), 2513−2525.
(63) Chandler, D. Statistical-Mechanics of Isomerization Dynamics in Liquids and Transition-State Approximation. *J. Chem. Phys.* **1978**, *68* (6), 2959−2970.
(64) Case, D. A.; Darden, T. A.; Cheatham, T. E., III; Simmerling, C. L.; Wang, J.; Duke, R. E.; Luo, R.; Merz, K. M.; Pearlman, D. A.; Crowley, M.; Walker, R. C.; Zhang, W.; Wang, B.; Hayik, S.; Roitberg, A.; Seabra, G.; Wong, K. F.; Paesani, F.; Wu, X.; Brozell, S.; Tsui, V.; Gohlke, H.; Yang, L.; Tan, C.; Mongan, J.; Hornak, V.; Cui, G.; Beroza, P.; Mathews, D. H.; Schafmeister, C.; Ross, W. S.; Kollman, P. A. *Amber 9*; University of California: San Francisco, 2006.
(65) Dang, L. X.; Chang, T. M. Molecular Dynamics Study of Water Clusters, Liquid, and Liquid-Vapor Interface of Water with Many-Body Potentials. *J. Chem. Phys.* **1997**, *106* (19), 8149−8159.
(66) Dang, L. X. Computational Study of Ion Binding to the Liquid Interface of Water. *J. Phys. Chem. B* **2002**, *106* (40), 10388−10394.
(67) Essmann, U.; Perera, L.; Berkowitz, M. L.; Darden, T.; Lee, H.; Pedersen, L. G. A Smooth Particle Mesh Ewald Method. *J. Chem. Phys.* **1995**, *103* (19), 8577−8593.
(68) Ryckaert, J. P.; Ciccotti, G.; Berendsen, H. J. C. Numerical-Integration of Cartesian Equations of Motion of a System with Constraints: Molecular-Dynamics of N-Alkanes. *J. Comput. Phys.* **1977**, *23* (3), 327−341.
(69) Dang, L. X.; Annapureddy, H. V. R. Computational Studies of Water Exchange around Aqueous $Li^+$ with Polarizable Potential Models. *J. Chem. Phys.* **2013**, *139* (8).
(70) Annapureddy, H. V.; Dang, L. X. Water Exchange Rates and Molecular Mechanism around Aqueous Halide Ions. *J. Phys. Chem. B* **2014**, DOI: 10.1021/jp500402j.
(71) Hertz, H. G. *Water: A Comprehensive Treatise*; Plenum Press: New York, 1973; Vol. 3.
(72) Geissler, P. L.; Dellago, C.; Chandler, D. Kinetic Pathways of Ion Pair Dissociation in Water. *J. Phys. Chem. B* **1999**, *103* (18), 3706−3710.
(73) Gai, H.; Dang, L. X.; Schenter, G. K.; Garrett, B. C. Quantum Simulation of Aqueous Ionic Clusters. *J. Phys. Chem.* **1995**, *99*, 13303. Gai, H.; Dang, L. X.; Schenter, G. K.; Garrett, B. C. Quantum Statistical Mechanical Simulation of the Ion−Water Cluster $I^-(H_2O)_n$: The Importance of Nuclear Quantum Effects and Anharmonicity. *J. Chem. Phys.* **1996**, *105*, 8835.
(74) Kuharski, R. A.; Rossky, P. J. A Quantum-Mechanical Study of Structure in Liquid $H_2O$ and $D_2O$. *J. Chem. Phys.* **1985**, *82*, 5164.
(75) Marx, D.; Tuckerman, M. E.; Parrinello, M. Solvated Excess Protons in Water: Quantum Effects on the Hydration Structure. *J. Phys.: Condens. Matter* **2000**, *12*, A153−A159.
(76) Vega, C.; Conde, M. M.; McBride, C.; Abascal, J. L. F.; Noya, E. G.; Ramirez, R.; Sese, L. M. Heat Capacity of Water: A Signature of Nuclear Quantum Effects. *J. Chem. Phys.* **2012**, *132*, 046101.
(77) Lobaugh, J.; Voth, G. A. The Quantum Dynamics of an Excess Proton in Water. *J. Chem. Phys.* **1996**, *104*, 2056.
(78) Habershon, S.; Manolopoulos, D. E.; Markland, T. E.; Miller, T. F. Ring-Polymer Molecular Dynamics: Quantum Effects in Chemical Dynamics from Classical Trajectories in an Extended Phase Space. *Annu. Rev. Phys. Chem.* **2013**, *64*, 387−413.
(79) Zhao, Z.; Rogers, D. M.; Beck, T. L. Polarization and Charge Transfer in the Hydration of Chloride Ions. *J. Chem. Phys.* **2010**, *132* (1), 014502.
(80) Varma, S.; Rempe, S. B. Multibody Effects in Ion Binding and Selectivity. *Biophys. J.* **2010**, *99* (10), 3394−3401.
(81) Soniat, M.; Rick, S. W. The Effects of Charge Transfer on the Aqueous Solvation of Ions. *J. Chem. Phys.* **2012**, *137* (4).
(82) Ballard, A. J.; Dellago, C. Toward the Mechanism of Ionic Dissociation in Water. *J. Phys. Chem. B* **2012**, *116* (45), 13490−13497.
(83) Mullen, R. G.; Shea, J.-E.; Peters, B. *J. Chem. Theory Comp.* **2014**, *10*, 659−667.
(84) Peters, B. Inertial Likelihood Maximization for Reaction Coordinates with High Transmission Coefficients. *Chem. Phys. Lett.* **2012**, *554*, 248−253.